Surface potential alignment in MoS₂ and MoTe₂ homo- and hetero-junctions

JIANG Cong[1,2], ZHANG Shuai-Jun[2], LI Yu-Ying[2,3], WANG Wen-Jing[2,4], XIA Hui[1,2,3*], LI Tian-Xin[2,3]

（1. College of Science, University of Shanghai for Science and Technology, Shanghai 200093, China;
2. State Key Laboratory of Infrared Physics, Shanghai Institute of Technical Physics, Chinese Academy of Sciences, Shanghai 200083, China;
3. University of Chinese Academy of Sciences, Beijing 100049, China;
4. Mathematics and Science College, Shanghai Normal University, Shanghai 200234, China）

Abstract：In transition metal dichalcogenides (TMD) flakes, the geometry, such as layer thickness, significantly tune the electronic properties, including bandgap, electron affinity and Fermi level. Such characteristic offers a high degree of freedom to tune the functionality of semiconductor device, once the volatile electronic properties are precisely determined. However, to date, there are still significant uncertainties in determining the Fermi-level alignment of TMD homo- or hetero- junctions, which might lead to significant deviations of band-bending and thus device performance. Here, we utilize the Scanning Kelvin Probe Microscopy (SKPM) to characterize the surface-potential/Fermi-level alignment of TMD homo- or hetero- junctions. Through this effort, a distinct phenomenon is verified where the Fermi-levels of MoS₂ and MoTe₂ shift towards the intrinsic level with an increasing layer thickness (in other words, the background doping concentration is continuously lowering). Moreover, we show the significant impact of surface contamination (molecular scale) on the surface potential of monolayer TMD. Finally, we fabricate a MoTe₂/MoS₂ heterojunction, in which we observe the wide depletion region and large photoresponse. Together, those findings might offer a reference to precisely stack van der Waals (vdW) layers as designed for both electronic and optoelectronic applications.

Key words：surface potential, transition metal dichalcogenides（TMD）, Scanning Kevin Probe Microscopy（SKPM）, layer thickness

MoS₂和MoTe₂同质结和异质结中的表面电势排列

江　聪[1,2]， 张帅君[2]， 李玉莹[2,3]， 王文静[2,4]， 夏　辉[1,2,3*]， 李天信[2,3]
（1. 上海理工大学 理学院，上海200093；
2. 中国科学院上海技术物理研究所 红外物理国家重点实验室，上海200083；
3. 中国科学院大学，北京100049；
4. 上海师范大学 数理学院，上海200234）

摘要：过渡金属硫族化合物(TMD)薄层仅改变几何形状(如层厚)就可调节带隙、电子亲和势和费米能级，使器件设计更灵活。但因缺乏费米能级排列信息，TMD同质/异质结器件常因未知的能带弯曲而偏离预期。利用扫描开尔文探针显微镜(SKPM)表征了TMD同质/异质结，结果显示，MoS₂和MoTe₂同质结的费米能级随层厚增加向本征费米能级移动(背景掺杂浓度降低)，而MoTe₂/MoS₂异质结中探测到宽耗尽区和强光响应，同时给出表面污染(分子尺度)对单层TMD表面电势的影响。上述发现将在器件设计中帮助精准堆叠范德华(vdW)层。

关　键　词：表面电势；过渡金属硫族化合物(TMD)；扫描开尔文探针显微镜(SKPM)；层厚

中图分类号：O472+.1　　**文献标识码**：A

Introduction

Transition metal dichalcogenides (TMD), a branch of two-dimensional (2D) layered materials, have attracted continuous attention from both academic and industrial societies due to their intriguing electronic and optoelectronic properties[1-4]. Generally, the bandgap, electron affinity and Fermi-level of layered TMD are tunable with a decreasing layer-thickness[5-9]. Moreover, each monolayer (ML) is connected by van der Waals force[10-12]. It spares TMD materials from surface states/charges and lattice mismatch, thus enabling a freewill stacking of heterostructures[13-14]. Both of these advantages lead to an extremely rich degree of freedom in designing and fabricating nanoscale electronic and optoelectronic devices. However, everything has two sides, the large-scale freedom also means enormous uncertainty in realistic device applications. In detail, the electronic characteristics of TMD materials, like the layer thickness dependent Fermi-level and band-bending, are still out of common sense[6,15]. For this reason, the fabricated homo- or hetero- structures usually deviate from the designed configuration. Note that the theoretical calculations can give a series of reference data[9,16-21]. However, as is well-documented, those results might deviate from the realistic situation[5,7,22], to a certain extent.

Scanning Kelvin Probe Microscopy (SKPM) has become a powerful tool for characterizing electronic properties in TMD, which are crucial for the design and optimization of TMD-based electronic and optoelectronic devices. Li et al. [23] and Feng et al. [24] characterized the surface potential variation of MoS_2 using SKPM under different substrates, light intensities, and humidity conditions. Robinson et al. [25] compared the surface potential of MoS_2 flakes exfoliated on substrates and suspended flakes using SKPM. Additionally, Wang et al. [26] utilized SKPM to reveal the work function change/Fermi level shift of WSe_2 as a function of gate voltage. Furthermore, Zhang et al. [27] confirmed the type-II energy band structure and interlayer charge separation in a $MoTe_2$/MoS_2 vdW heterostructure using SKPM. Overall, SKPM provides a non-destructive and high-resolution method for characterizing TMD materials, which could facilitate the development of TMD-based electronic and optoelectronic devices.

In this work, SKPM method is utilized to characterize the surface potential of TMD materials, MoS_2 and $MoTe_2$. As a result, a distinct phenomenon has been observed, in which the Fermi-level (E_F) of MoS_2 and $MoTe_2$ shifts toward the intrinsic level (E_i) with an increasing layer thickness. It indicates that the background doping concentrations of TMD materials are decreasing continuously. These characteristics should be associated with the band structure reconstruction process, in which the formation energy of the intrinsic dopants changes obviously. Finally, we show the alignment of Fermi-level in a typical MoS_2/$MoTe_2$ heterostructure and the effect of light illumination on it. The findings disclosed here might provide key information for the design and fabrication of van der Waals devices.

1 Experiments

Homogeneous structures of $MoTe_2$ and MoS_2 flakes were mechanically exfoliated onto a silicon substrate covered with a 280 nm-thick thermal oxide layer. To obtain $MoTe_2$/MoS_2 heterostructures, MoS_2 monolayers were first deposited on Si/SiO_2 substrate by chemical vapor deposition (CVD) and a single layer $MoTe_2$ was subsequently transferred onto a selected monolayer of MoS_2. All samples were tested in a nitrogen atmosphere to reduce the influence of water and adsorbates, in order to characterize the intrinsic electrical properties of the materials.

A Bruker icon scanning probe microscope with Nanoscope IV controller is used in the experiment. Probes with n-doped Si were selected for both topography and surface potential measurement. We identified thin layers of MoS_2 and $MoTe_2$ using an optical microscope, and then used atomic force microscopy (AFM) to characterize the film thickness. The amplitude modulation mode (AM-mode) SKPM was performed to investigate the band alignment of homo- and hetero- structures formed by $MoTe_2$ and MoS_2. To explore the interlayer photoexciting effect on $MoTe_2$/MoS_2 type-II heterostructures, we performed SKPM analysis under dark and illuminated conditions, with a laser wavelength of 680 nm.

2 Results and discussions

Figures 1(a) and 1(c) show the AFM image and height profile of MoS_2 flake that was mechanically exfoliated and transferred onto a Si/SiO_2 substrate. The stepped topography helps to identify five distinct layer-thicknesses, namely 1L, 2L, 3L, 4L, and 6L MoS_2. The corresponding SKPM image and potential profile are shown in Figs. 1(b) and (d). One can find that each increase in layer thickness (monolayer's level) would lead to a decrease of surface potential, from 2.2 meV @1L to -8.2 meV @2L, -18 meV @4L and finally -20.3 meV @6L.

It was once thought that oxygen and moisture in the environment would change the surface potential[6], thus responsible for the variable SKPM-signal with an increasing layer thickness. However, in our experiments, all samples were tested in a nitrogen atmosphere to minimize the influence of adsorbates (such as oxygen and water molecules) on the intrinsic electrical properties of TMD. Furthermore, as shown in Fig. 2(c), we observe an opposite trend of the evolution of surface potential in $MoTe_2$ flake, which cannot be explained by the above-mentioned reasons (which predicts a monotonic relationship between potential and layer thickness that is independent of the material category).

Here, we attribute the phenomenon in Figs. 1(c) and 1(d) to the intrinsic variation of the Fermi level. This is because the band structure of van der Waals materials is reconstructed with an increasing layer thickness. It could strongly tune the background doping property, e. g. by altering the defect forming energy. Figure 1(e) compares the bandgap with the surface potential at different layer thicknesses. One can find that both characters
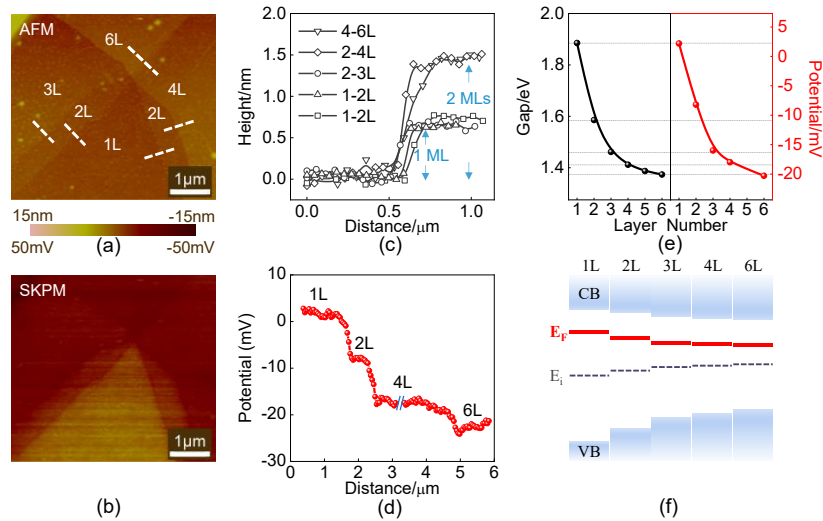
Fig. 1   The SKPM experimental results of few-layer MoS$_2$ (a) the AFM image of stepped MoS$_2$, including 1L，2L，3L ，4L and 6L，(b) the SKPM image of the corresponding topography of MoS$_2$，(c) the MoS$_2$ height profile corresponding to the white dashed line marked in (a)，(d) the surface potential distribution of few-layer MoS$_2$ extracted from (b)，(e) the bandgap and potential of MoS$_2$ as a function of layer thickness，in black and red，respectively (the bandgap data are from the theoretical calculation results in Ref. 5)，the potential data at 6L are regional average，(f) evolution of the Fermi level of MoS$_2$ with different layers
图 1   少层 MoS$_2$ 的 SKPM 实验结果 (a) 台阶状 MoS$_2$ 的 AFM 图像，包括 1 层，2 层，3 层，4 层和 6 层，(b) MoS$_2$ 对应形貌的 SKPM 图像，(c) (a) 中白色虚线对应的 MoS$_2$ 高度曲线，(d) (b) 中提取的少层 MoS$_2$ 的表面电势分布，(e) MoS$_2$ 的带隙和电势随层厚的依赖关系，分别用黑色和红色表示，(f) MoS$_2$ 费米能级随层厚的演变

follow the same trend of evolution，which might be the direct evidence to support the judgement.

To further test this，we performed the SKPM experiment on another TMD material，MoTe$_2$. The typical result is shown in Fig. 2. The morphology image (Fig. 2 (a)) helps to identify three distinct regions，1L，2L and 3L MoTe$_2$. Correspondingly，the surface potential exhibits an obvious enhancement in the thick-layer counterpart

of MoTe$_2$ (Fig. 2(b)). It is contrary to that of MoS$_2$，where the potential increases with an increasing layer thickness. Figures 1(f) and 2(e) schematically show the band structures of MoS$_2$ and MoTe$_2$，respectively. The Fermi-level is carefully labelled to show the opposite evolution processes.

It is worth noting that there are space charge regions (SCR) in the MoTe$_2$ sample，especially at the 1L/2L and
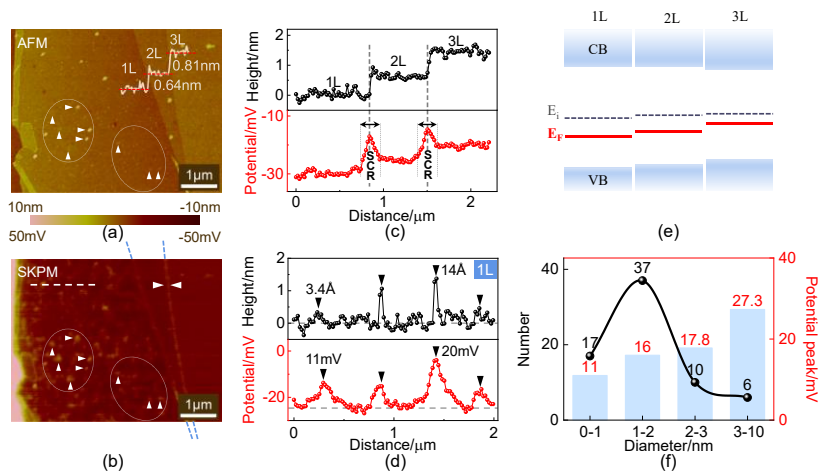

Fig. 2   The SKPM experimental results of few-layer MoTe$_2$ (a) the AFM image of stepped MoTe$_2$，including 1L，2L and 3L，(b) the SKPM image of the corresponding topography of MoTe$_2$，the light blue dashed lines are extensions of the potential boundary，The white triangles in white dashed ovals mark topography and potentials due to the module absorption or contamination，(c) the surface potential distribution and corresponding topography of the few-layer MoTe$_2$ extracted from (a) and (b)，(d) the height and potential curves corresponding to the white dotted line in the MoTe$_2$ monolayer region in (b)，(e) evolution of the Fermi level of MoTe$_2$ with different layers，(f) the number and average potential of adsorbates with different diameter ranges in the monolayer region of MoTe$_2$
图 2   少层 MoTe$_2$ 的 SKPM 实验结果 (a) 台阶状 MoTe$_2$ 的 AFM 图像，包含 1 层，2 层和 3 层，(b) MoTe$_2$ 对应形貌的 SKPM 图像，浅蓝色虚线是电势边界的延长线，白色虚线椭圆内部的白色三角标记了由模块吸收和污染导致的形貌和电势，(c) (a) 和 (b) 中提取的少层 MoTe$_2$ 对应形貌的表面电势分布，(d) (b) 中 MoTe$_2$ 单层区域白色虚线对应的高度和电势曲线，(e) MoTe$_2$ 费米能级随层厚的演变，(f) MoTe$_2$ 单层区域吸附物不同直径范围的数量和平均电势

2L/3L interfaces（Fig. 2（b）, marked by white triangles and blue dashed lines）. It arises from the band offset between different layer-thickness regions, which can be defined as the depletion region of the layer junction. Such a characteristic is much more obvious in $MoTe_2$, but almost invisible in MoS_2. The difference in charge carrier concentration might be responsible for the phenomenon. In detail, $MoTe_2$ is lightly p-doped（a well-known bipolar material）[28-30], MoS_2 is heavily n-doped[31-32]. Thus, the depletion region of $MoTe_2$ could be ordered wider than that of MoS_2.

Another interesting phenomenon is that the fluctuations of surface potential are clearly recorded in our SKPM experiments（Fig. 2（b））, even if they are sub-nanometer scale and originate from molecules absorption or contamination. As shown in Figs. 2（b）and 2（d）, in the monolayer $MoTe_2$ region, there is a high density of potential fluctuation（as high as 20 meV）, which arises from the sub-nanometer molecules that are incorporated during the mechanical exfoliation process. Figure 2（f）shows a statistical analysis on the diameter and potential of the adsorbed molecules or molecule clusters in the monolayer $MoTe_2$. One can find that the diameter of molecular clusters spans from sub-nanometer to 10 nanometers; the most frequently found molecules are sub-2 nm ones, which account for 77% of the whole community. The histogram plot shows the relation between the potential fluctuations on the scale of absorbed molecule. It makes sense that the potential fluctuation rises from 11 meV to 27 meV with an increase of the molecule diameter.

Furthermore, we prepared a 1L $MoTe_2$-1L MoS_2 heterostructure. As depicted in Fig. 3（a）, the sample was fabricated by transferring a monolayer $MoTe_2$ onto the 1L-MoS_2. In SKPM experiments, the $MoTe_2$ film shows a 104 mV drop in potential. It indicates that the 1L $MoTe_2$-1L MoS_2 heterostructure is a typical pn junction. At the same time, the SKPM experiment helps to identify the depletion region of such vdW hetero-junction. As shown in Fig. 3（c）, the transition region between n-MoS_2 and p-$MoTe_2$ is a classic space charge region. Its width is as large as 750 nm. A more detailed analysis confirms this conclusion. Figure 3（d）plots the dependence of potential drop on the width of $MoTe_2$ strip. One can find that the potential drop increases significantly（58 to 109 mV）as the $MoTe_2$ width increases from 350 to 750 nm. In this specific region, the $MoTe_2$ layer is fully depleted, thus the potential drop is highly dependent on the layer width. By contrast, when the $MoTe_2$ width is over 750 nm, the potential drop is constant. It implies that the junction cannot deplete more material. The 750 nm should be the final width of the depletion region. It is also worth noting that such vdW hetero-junction shows a significant response to light illumination[27], since the potential drop increases by ~20 mV.

3 Conclusions

We explore the effect of layer thickness on the band alignment of homo- and hetero-structures formed by few-
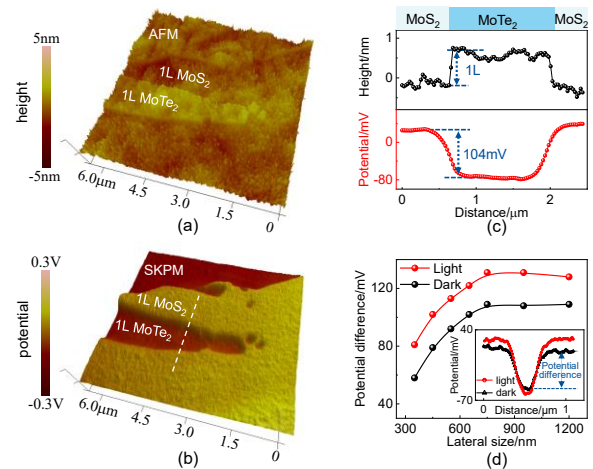

Fig. 3 The SKPM experimental results of $MoTe_2$/MoS_2 vdW heterostructures（a）the AFM 3D image of $MoTe_2$/MoS_2 vdW heterostructure,（b）the SKPM 3D image of corresponding topography,（c）the topography and surface potential distributions corresponding to the white dashed line in（b）,（d）the size dependence of the potential difference between the $MoTe_2$/MoS_2 vdW heterojunction and MoS_2 under dark and light conditions, the inset shows the changes in surface potential of the $MoTe_2$/MoS_2 heterostructure under dark and light conditions

图 3 $MoTe_2$/MoS_2 异质结构的 SKPM 实验结果（a）$MoTe_2$/MoS_2 异质结构的三维 AFM 图像,（b）对应形貌的三维 SKPM 图像,（c）对应（b）中白色虚线的形貌和电势分布,（d）黑暗和光照条件下 $MoTe_2$/MoS_2 异质结和 MoS_2 之间电势差的尺寸依赖性,插图展示了 $MoTe_2$/MoS_2 异质结构的表面电势在黑暗和光照条件下的变化

layer MoS_2 and $MoTe_2$. As the layer thickness increases, the Fermi level of MoS_2 decreases while the Fermi level of $MoTe_2$ increases, resulting in opposite evolution trends. The observed space charge region in $MoTe_2$ is attributed to differences in carrier concentrations, while significant surface potential fluctuations in the monolayer region reveal the effects of impurity adsorbents and nonideal storage conditions. Our findings offer guidance for the fabrication of 2D material-based devices. We also prepared a vdW heterostructure of monolayers MoS_2 and $MoTe_2$, and observed a classical space charge region with a final depletion region width of 750 nm. The potential drop of the vdW heterostructure increased by 20 mV under illumination, indicating a good photo-response.

In summary, this work expands our understanding of the electronic structure of layered TMD materials, demonstrating that band alignment can be modified by adjusting the layer thickness. This property likely extends to other TMD materials, offering important guidance for the design of next-generation electronic and optoelectronic devices based on TMD homo- or hetero-structures.

References

［1］Tan C L, Lai Z C, Zhang H. Ultrathin Two-Dimensional Multinary Layered Metal Chalcogenide Nanomaterials［J］. *Advanced Materials*, 2017, **29**(37): 1701392.

［2］Xie C, Mak C, Tao X M, *et al*. Photodetectors Based on Two-Dimensional Layered Materials Beyond Graphene［J］. *Advanced Functional Materials*, 2017, **27**(19): 1603886.

［3］Bhimanapati G R, Lin Z, Meunier V, *et al*. Recent Advances in Two-Dimensional Materials beyond Graphene［J］. *Acs Nano*, 2015,

9(12)：11509−11539.

[4] Bao X Z, Ou Q D, Xu Z Q, *et al*. Band Structure Engineering in 2D Materials for Optoelectronic Applications [J]. *Advanced Materials Technologies*, 2018, **3**(11)：1800072.

[5] Mak K F, Lee C, Hone J, *et al*. Atomically Thin MoS$_2$: A New Direct−Gap Semiconductor [J]. *Physical Review Letters*, 2010, **105** (13)：136805.

[6] Li Y, Xu C Y, Zhen L. Surface potential and interlayer screening effects of few−layer MoS$_2$ nanoflakes [J]. *Applied Physics Letters*, 2013, **102**(14)：143110.

[7] Ruppert C, Aslan O B, Heinz T F. Optical Properties and Band Gap of Single− and Few−Layer MoTe$_2$ Crystals [J]. *Nano Letters*, 2014, **14**(11)：6231−6236.

[8] Kim H G, Choi H J. Thickness dependence of work function, ionization energy, and electron affinity of Mo and W dichalcogenides from DFT and GW calculations [J]. *Physical Review B*, 2021, **103**(8)：085404.

[9] Lee H, Deshmukh S, Wen J, *et al*. Layer−Dependent Interfacial Transport and Optoelectrical Properties of MoS$_2$ on Ultraflat Metals [J]. *Acs Applied Materials & Interfaces*, 2019, **11**(34)：31543−31550.

[10] Geim A K, Grigorieva I V. Van der Waals heterostructures [J]. *Nature*, 2013, **499**(7459)：419−425.

[11] Novoselov K S, Mishchenko A, Carvalho A, *et al*. 2D materials and van der Waals heterostructures [J]. *Science*, 2016, **353**(6298)：aac9439.

[12] Das S, Chen H Y, Penumatcha A V, *et al*. High Performance Multilayer MoS2 Transistors with Scandium Contacts [J]. *Nano Letters*, 2013, **13**(1)：100−105.

[13] Li M Y, Chen C H, Shi Y M, *et al*. Heterostructures based on two−dimensional layered materials and their potential applications [J]. *Materials Today*, 2016, **19**(6)：322−335.

[14] Zheng W H, Zheng B Y, Yan C L, *et al*. Direct Vapor Growth of 2D Vertical Heterostructures with Tunable Band Alignments and Interfacial Charge Transfer Behaviors [J]. *Advanced Science*, 2019, **6**(7)：1802204.

[15] Xia H, Luo M, Wang W J, *et al*. Pristine PN junction toward atomic layer devices [J]. *Light−Science & Applications*, 2022, **11**(1)：170.

[16] Cheiwchanchamnangij T, Lambrecht W R L. Quasiparticle band structure calculation of monolayer, bilayer, and bulk MoS$_2$ [J]. *Physical Review B*, 2012, **85**(20)：205302.

[17] Boker T, Severin R, Muller A, *et al*. Band structure of MoS$_2$, MoSe$_2$, and alpha−MoTe$_2$: Angle−resolved photoelectron spectroscopy and ab initio calculations [J]. *Physical Review B*, 2001, **64**(23)：235305.

[18] Kang J, Tongay S, Zhou J, *et al*. Band offsets and heterostructures of two−dimensional semiconductors [J]. *Applied Physics Letters*, 2013,

102(1)：012111.

[19] Hu W D, Ye Z H, Liao L, et al. 128 x 128 long−wavelength/mid−wavelength two−color HgCdTe infrared focal plane array detector with ultralow spectral cross talk [J]. *Optics Letters*, 2014, **39**(17)：5130−5133.

[20] Gong C, Zhang H J, Wang W H, *et al*. Band alignment of two−dimensional transition metal dichalcogenides: Application in tunnel field effect transistors [J]. *Applied Physics Letters*, 2013, **103**(5)：053513.

[21] Hu W D, Chen X S, Ye Z H, et al. A hybrid surface passivation on HgCdTe long wave infrared detector with in−situ CdTe deposition and high−density Hydrogen plasma modification [J]. *Applied Physics Letters*, 2011, **99**(9)：091101.

[22] Mcdonnell S, Azcatl A, Addou R, *et al*. Hole Contacts on Transition Metal Dichalcogenides: Interface Chemistry and Band Alignments [J]. *Acs Nano*, 2014, **8**(6)：6265−6272.

[23] Li F, Qi J J, Xu M X, *et al*. Layer Dependence and Light Tuning Surface Potential of 2D MoS$_2$ on Various Substrates [J]. *Small*, 2017, **13**(14)：1603103.

[24] Feng Y L, Zhang K L, Li H, *et al*. In situ visualization and detection of surface potential variation of mono and multilayer MoS$_2$ under different humidities using Kelvin probe force microscopy [J]. *Nanotechnology*, 2017, **28**(29)：295705.

[25] Robinson B J, Giusca C E, Gonzalez Y T, *et al*. Structural, optical and electrostatic properties of single and few−layers MoS$_2$: effect of substrate [J]. *2d Materials*, 2015, **2**(1)：015005.

[26] Wang Z G, Li Q, Chen Y F, *et al*. The ambipolar transport behavior of WSe$_2$ transistors and its analogue circuits [J]. *Npg Asia Materials*, 2018, **10**(8)：703−712.

[27] Zhang K N, Zhang T N, Cheng G H, *et al*. Interlayer Transition and Infrared Photodetection in Atomically Thin Type−II MoTe$_2$/MoS$_2$ van der Waals Heterostructures [J]. *Acs Nano*, 2016, **10**(3)：3852−3858.

[28] Pezeshki A, Hossein S, Shokouh H, *et al*. Electric and Photovoltaic Behavior of a Few−Layer alpha−MoTe$_2$/MoS$_2$ Dichalcogenide Heterojunction [J]. *Advanced Materials*, 2016, **28**(16)：3216−3222.

[29] Lin Y F, Xu Y, Wang S T, *et al*. Ambipolar MoTe$_2$ Transistors and Their Applications in Logic Circuits [J]. *Advanced Materials*, 2014, **26**(20)：3263−3269.

[30] Fathipour S, Ma N, Hwang W S, *et al*. Exfoliated multilayer MoTe$_2$ field−effect transistors [J]. *Applied Physics Letters*, 2014, **105**(19)：192101.

[31] Radisavljevic B, Radenovic A, Brivio J, *et al*. Single−layer MoS$_2$ transistors [J]. *Nature Nanotechnology*, 2011, **6**(3)：147−150.

[32] Liu H Q, Ba K, Gou S F, *et al*. Reversing the Polarity of MoS$_2$ with PTFE [J]. *Acs Applied Materials & Interfaces*, 2021, **13**(38)：46117−46124.